55-330

NASA

Technical Memorandum 83822

VISSR ATMOSPHERIC SOUNDER (VAS) SIMULATION EXPERIMENT FOR A SEVERE STORM ENVIRONMENT

Dennis Chesters, Louis W. Uccellini
and Anthony Mostek

SEPTEMBER 1981

National Aeronautics and
Space Administration

Goddard Space Flight Center
Greenbelt, Maryland 20771

VISSR ATMOSPHERIC SOUNDER (VAS) SIMULATION EXPERIMENT FOR A SEVERE STORM ENVIRONMENT

Dennis Chesters and Louis W. Uccellini
Codes 915 and 914
Goddard Laboratory for Atmospheric Sciences (GLAS)
Greenbelt, MD 20771

and

Anthony Mostek
Computer Sciences Corporation
Silver Spring, MD 20910

August 10, 1981

GODDARD SPACE FLIGHT CENTER
Greenbelt, Maryland 20771

ABSTRACT

The GOES satellites launched in the 1980s are carrying an instrument called the VISSR Atmospheric Sounder (VAS), which is designed to provide temperature and moisture profile sounding capability for mesoscale weather systems. As a prelaunch study of this capability, VAS radiance fields are simulated for pre-thunderstorm environments in Oklahoma to demonstrate three points: (1) significant moisture gradients can be seen directly in images of the VAS channels, (2) temperature and moisture profiles can be retrieved from VAS radiances with sufficient accuracy to be useful for mesoscale analysis of a severe storm environment, and (3) the quality of VAS mesoscale soundings improves with conditioning by local weather statistics.

Even though the simulated VAS soundings have the usual limitations in absolute accuracy and vertical resolution (especially in the lower tropospheric moisture retrievals), it is still possible to discern potentially unstable mesoscale structures from the synthetic VAS radiances for a partly cloudy pre-thunderstorm environment. The RMS tropospheric profile errors are ±1° C and ±25 percent in temperature and mixing ratio, respectively. The results represent the optimum retrievability of mesoscale information from VAS radiances without the use of ancillary data. The simulations suggest that VAS data will yield the best soundings when a human being classifies the scene, picks relatively clear areas for retrieval, and applies a "local" statistical data-base to resolve the ambiguities of satellite observations in favor of the most probable atmospheric structure.

TABLE OF CONTENTS

	Page
ABSTRACT	iii
1. INTRODUCTION	1
2. DESCRIPTION OF VAS	3
2.1 The VAS Instrument	4
2.2 VAS Channel Sensitivities	4
3. EXPERIMENT DESIGN	6
3.1 NSSL Database	7
3.2 Statistical Design	7
4. VAS RADIANCE SIMULATION	8
4.1 Radiation Transfer	9
4.2 Simulated VAS Images	9
4.3 Correlation Between Moisture and VAS Radiances	10
5. RESIDUAL ERRORS IN SIMULATED VAS SOUNDINGS	11
5.1 Conditioned Regression Retrievals	11
5.2 "Local" vs. "Global" Retrieval Quality	13
5.3 Fine Tuning the "Local" Retrieval Statistics	14
5.4 Retrieval of Vertically Integrated Parameters	15
6. MESOSCALE ANALYSIS OF VAS SIMULATED SOUNDINGS	16
6.1 Analysis of Horizontal Cross Sections	17
6.2 Analysis of Vertical Cross Sections	18
6.3 Analysis of Integrated Parameters	19
7. SUMMARY AND DISCUSSION	21
ACKNOWLEDGEMENTS	24
REFERENCES	25

LIST OF TABLES

Page

Table 1. Prelaunch specifications for the 12 VAS channels, all of which have 15 km (nadir view) resolution. 27

Table 2. Estimated sensitivity of the VAS channels for nadir view simulations of the U.S. Standard Atmosphere and a set of 32 "globally" distributed radiosondes. 28

Table 3. The NSSL6 datasets used to "locally" condition regression matrices for simulated VAS soundings. 29

Table 4. The NSSL4 datasets used to test simulated VAS soundings. The four frames are drawn from the initial and developing stages of two well observed storms. The frame at 2030 GMT 29 May 1976 is used to simulate VAS images. 30

Table 5. Mean and standard deviations of precipitable water and geopotential thickness from the NSSL4 test set for the "ground truth" profiles and residual errors in the "global" and "local" retrievals. 31

LIST OF ILLUSTRATIONS

Figure		Page
1	VAS weighting functions for the seven temperature sounding channels	32
2	VAS weighting functions for the three moisture sounding and two window channels	33
3	SMS 11 micron image on 29 May 1976 at 2030 GMT with an overlay of the 21 x 11 Barnes analysis grid at 20 km resolution for simulated VAS images and an imbedded 7 x 5 grid at 50 km resolution for simulated soundings	34
4	Synthetic VAS brightness temperature images for a pre-storm environment at 2030 GMT 29 May 1976 using the 20 km analysis grid and SMS cloud estimates	35
5	"Split window" brightness temperature differences plotted against the corresponding low level moisture for all 210 SFOVs in the NSSL6 dependent training frames	38
6	RMS temperature residuals (simulated sounding – "ground truth"), where VAS retrievals were statistically conditioned to expect vertical structure determined by either: (△) the "global" NOAA32 or (□) the "local" NSSL6 radiosonde sets	39
7	RMS mixing ratio residuals, where VAS retrievals were statistically conditioned to expect vertical structure determined by either: (△) the "global" NOAA32 or (□) the "local" NSSL6 radiosonde sets	40
8	RMS temperature residuals using: (□) all, (△) "wet" and (○) "dry" SFOVs from the "local" NSSL6 training set to test even more detailed statistical conditioning of the simulated VAS soundings	41
9	RMS mixing ratio residuals using: (□) all, (△) "wet" and (○) "dry" SFOVs from the "local" NSSL6 training set to test even more detailed statistical conditioning of the simulated VAS soundings	42
10	NWS surface analysis depicting pressure (mb) and dewpoint temperature (°F) at 0000 GMT 30 May 1976	43

VISSR ATMOSPHERIC SOUNDER (VAS) SIMULATION EXPERIMENT FOR A SEVERE STORM ENVIRONMENT

1. INTRODUCTION

Present atmospheric soundings from operational satellites are designed for the collection of temperature and humidity data for global analysis and for input to numerical models that simulate the large-scale general circulation. The soundings are performed from sun-synchronous polar orbiting satellites, which provide complete coverage of the globe with a spatial scale of several hundred kilometers twice per day per satellite. The entire system, which includes the sounders on the satellites, the algorithms for reducing the data and retrieving the desired atmospheric variables, and the general circulation models, is aimed at improving the intermediate-to long-range forecasts of the large-scale circulation patterns.

The need for understanding short-lived weather phenomena, such as severe local storms, and the growing requirements for more accurate local weather forecasts that require atmospheric data with a finer spatial scale and more frequent observations point toward a different satellite system: one centered around soundings from a geosynchronous platform. Severe local storm research and prediction require frequent observations at subsynoptic to mesoscale resolution in order to capture the relevant changes in the atmospheric mass and wind fields. The incorporation of ancillary data (e.g., conventional surface and radiosonde reports) from the meteorologically active areas is expected to become an important aid to the satellite sounding process. Likewise, an understanding of the physics of the phenomenon under observation should be helpful in modeling the radiation transfer for the retrieval algorithms.

The VISSR Atmospheric Sounder (VAS), which is now operating as an integral part of the Geostationary Operational Environmental Satellite (GOES) system, is designed to meet the requirements of observing subsynoptic to mesoscale temperature and moisture distributions. Ultimately, the goal is to observe, understand and predict the development of severe storms. The geosynchronous VAS will watch the development of mesoscale weather systems, typically surveying the United States with 12 spectral bands once per hour at 15 km (nadir view) resolution. Satellite

soundings derived from such multispectral scenes will have 30 to 90 km effective resolution, since several pixels must be used to average radiometric noise and to deal with broken cloud cover in the net sounding field of view (SFOV).

At this time, the polar orbiting satellite sounders are operationally useful over the data-sparse oceans where both the underlying uniformity of the ocean surface and the passive microwave data are important data processing aids for synoptic scale retrievals. These soundings show some systematic error patterns, such as larger errors near the surface and tropopause, biased performance in partly cloudy areas, and low sensitivity to horizontal gradients (Phillips, *et. al.*, 1979).

Operational satellite soundings over land have similar errors: the subsynoptic gradients are underestimated, and there are significant errors where the underlying topography is unusual or persistently cloudy (Schlatter, 1981). Operational satellite soundings are usually ignored in favor of the conventional radiosonde network, despite the inadequate space-time resolution of the conventional synoptic data for mesoscale developments. Case studies over mesoscale networks with satellite radiances from the Vertical Temperature Profile Radiometer (VTPR) have been encouraging. VTPR retrievals at 70 km resolution over the Atmospheric Variability Experiment (AVE) produce temperature fields and precipitable water estimates comparable to the AVE data (Hillger and Vonder Haar, 1977). VTPR radiance correlations over the National Severe Storms Laboratory (NSSL) network show spatial structure comparable to the meteorological correlations in the NSSL analyses, although the retrieved moisture information is not well determined (Hillger and Vonder Haar, 1979).

Polar orbiting sounder studies are hampered by the lack of unambiguous, independent, colocated "ground truth" data, taken with space-time resolution as good as the satellite observations. This VAS simulation study avoids these problems by declaring that selected mesoscale profile analyses are "ground truth," and then retrieving profiles from corresponding synthetic radiance fields so that unambiguous estimates of retrieval accuracy can be made. The quantitative results provide a benchmark for mesoscale retrieval accuracy available from the VAS sounder for optimal sounding conditions without help from ancillary data or from physically modeled retrieval algorithms.

This paper describes a simulation experiment designed to estimate the accuracy of VAS soundings within a severe weather environment, given cloud-free observing conditions. The pre-launch experiment is specifically designed to determine:

1. Whether moisture gradients can be seen directly with the VAS images,
2. Whether temperature and moisture profiles and gradients can be retrieved from VAS radiances with sufficient accuracy to be useful for mesoscale analysis of a severe storm environment,
3. Whether the quality of VAS soundings improve with conditioning by local weather statistics.

A brief summary of the VAS instrument and the VAS channels is provided in section 2. The experiment is defined in section 3. Simulated imagery results are discussed in section 4 with a statistical analysis of the soundings presented in section 5. The application of VAS soundings in the analysis of precursor conditions for severe convective storms is presented in section 6, and a discussion of the results follows in section 7.

2. DESCRIPTION OF VAS

During the 1970s, the Visible Infrared Spin Scan Radiometer (VISSR) was carried on the SMS/GOES series of geosynchronous satellites. VISSR infrared images in the 11 micron window are formed by stepping the scan line each spin by its own width (7 km resolution at nadir). During the 1980s, the GOES satellites will carry an upgraded instrument called the VISSR Atmospheric Sounder (VAS). The VAS instrument has programmable features which allow a ground-based operator to interact with the satellite by using the most recent observations to command when, where and how VAS will acquire data. The user will be limited only by the available time, filter/detector combinations and radiometric constraints (see Table 1 at the end of this technical memorandum). The geosynchronous location can be exploited to observe the development of mesoscale weather systems. For example, VAS can take sounding quality (low noise) radiances at 15 km (nadir view) resolution along a full earth east-west swath with a north-to-south extent large

enough to cover Oklahoma every 20 minutes or with a north-to-south extent large enough to cover the conterminous United States every hour.

2.1 *The VAS Instrument*

VAS has 12 thermal infrared channels between 4 and 15 microns. The channels are chosen to distinguish the effects of tropospheric temperature, moisture and cloud cover upon the upwelling radiances. All 12 channels can be operated at 15 km resolution (instantaneous geometrical field of view at nadir), and channels 4, 5, 7, 8, 9 and 10 can be operated at 7 km resolution. (The other channels are too noise- or diffraction-limited to be operated at higher resolution.) The VISSR radiometer has been upgraded to yield high precision values (10 bits) from six detectors, carefully calibrated with outer space (3° K) and an internal hot target (320° K). Radiometric noise is reduced by "dwell averaging" several spins on the same line and channel; the number of spins allocated to the channels is termed the "spin budget." Noise can also be reduced after data collection by judicious averaging of the clear adjacent fields of view.

Table 1 summarizes key design features of the 12 VAS channels: central wavelength, wavenumber and bandpass; purpose for sounding; main absorbing gasses and other important influences; single-sample noise; radiometric noise requirements for sounding; and a nominal spin budget for dwell averaging each channel. Lower spin budgets can be used to trade radiometric accuracy for speed and latitude coverage. In that case, pixel averaging of the 15 km (nadir view) instantaneous geometrical fields of view (IGFOVs) into, say, a 60 km sounding field of view (SFOV) is possible to regain radiometric accuracy at the expense of detailed resolution. Nominal calibration specifications are ±1.5° K absolute and ±0.5° K relative brightness temperature ΔT^* in all channels for a typical earth scene. For comparison, the previous VISSR instrument had calibration errors of roughly ±3° K.

2.2 *VAS Channel Sensitivities*

VAS transmission functions, $\tau(\nu, p)$, are computed for each channel (designated with wavenumber ν) at 40 pressure levels p, from .2 to 1000 mb. The transmissions are done for CO_2, N_2,

N_2O, NO, CH_4, O_2, plus H_2O, using line-by-line absorption coefficients (McClatchey, *et. al.*, 1973) and important molecular continuum absorption cross sections (Burch, *et. al.*, 1970-1; Roberts, *et. al.*, 1976). Corresponding weighting functions, d τ/dln P, are shown for the U.S. Standard Atmosphere in Figure 1, which is presented at the end of this technical memorandum, for the temperature sounding channels and in Figure 2 for the moisture and window channels. The short wave channels are indicated with dashed lines. The redundancy between the long and short wave channels will be used to detect cloud contamination by exploiting the differential sensitivity of the Planck function to cloud-top temperature. The sharp peaks of the moisture channels in Figure 2 are related to the exponential average distribution of water vapor. Consequently, the altitude of their peak response is not very predictable, since the radiance accumulates from only the top few millimeters of the total water burden.

Figures 1 and 2 show that the lower troposphere (500 to 1000 mb) is not well resolved by any one of the VAS channels. The radiation from the temperature and moisture structures just above the boundary layer (700 to 900 mb) is mixed with both surface and mid-tropospheric radiances in all the key VAS channels (5 to 8 and 12). The "man in the loop" concept will be an important factor to successful sounding with VAS (Smith, *et. al.*, 1978) where radiances will be confused by low clouds, topography and irregular surface emission. Also, the inclusion of surface temperature and moisture information into the retrieval scheme can be of great value in properly determining the atmospheric boundary conditions (Hayden, 1980). This prelaunch sounding experiment will test whether the lower tropospheric VAS channels can independently detect potentially unstable temperature and moisture structures using simulated clear column radiances over a featureless level surface which is thermally coupled to the bottom of the troposphere.

Table 2 summarizes some calculated responses of the VAS channels to the clear atmosphere: the pressure level of the peak of each standard weighting function; the pressure range over which the middle 80 percent of the radiance accumulates; the net sensitivity of the brightness temperature to a 1° C increase in the entire air temperature profile or in the dewpoint profile or in the

surface temperature alone; mean and standard deviations of VAS simulated brightness temperatures for a set of 32 radiosondes distributed over North America; and "signal"/noise estimates made by comparing these variances to the single-sample noise listed in Table 1. Roughly speaking, the "signal" (variance) in the tropospheric channels is 5 percent of the total brightness, and the noise is 0.5 percent giving a "signal"/noise of about 10 to 1.

The net sensitivity estimates in Table 2 suggest simple channel combinations for special environments. One promising combination is VAS channels 7 and 8, which form a "split window" for water vapor determination in the lower troposphere, since the two channels have different sensitivity to moisture variations at nearly the same wavelength (Prabhakara, *et. al.*, 1974). For instance, a SFOV with 5° C higher dewpoint than the U.S. Standard will appear 1.8° K colder at 12 microns due to the increased absorption by water vapor, but only 1.0° K colder at 11 microns. Consequently, this "split window" should be able to directly display horizontal moisture gradients, such as pre-thunderstorm "dryline" environments with warm dry air next to cool moist air.

3. EXPERIMENT DESIGN

The VAS simulation experiment is designed to determine the potential accuracy of VAS temperature and moisture retrievals within a realistic severe weather environment and the sensitivity of these retrievals to localized statistical conditioning.

Since VAS will be directed to take radiance observations over a developing mesoscale event (e.g., thunderstorm or hurricane), the VAS sounding algorithms should be prepared to take advantage of the information implicit in the classification of the scene by the VAS user. This study demonstrates the retrieval advantage enjoyed by a user who has prepared for pre-thunderstorm soundings by the use of objective statistics gathered from previous mesoscale radiosonde analyses. While it is difficult to quantify the accuracy of a human classification, one can measure the post-classification retrieval advantage by comparing soundings made with appropriate "local" training to soundings made with unselective "global" training.

3.1 *NSSL Database*

Temperature and moisture profiles for eight severe local storm events were selected from the radiosonde network operated by the National Severe Storm Laboratory (NSSL) in 1976 (see Tables 3 and 4) to be utilized for VAS radiance simulations. The storm environments range from mild to chaotic gradients, most having "dryline" characteristics with weak temperature gradients but strong moisture gradients (Mostek, *et. al.*, 1980). Ten different "frames" (times) were analyzed from the eight events, so that each frame could be used to simulate corresponding VAS radiance observations. The events were generally analyzed early in the storm development, which are relatively cloud-free, representing times when the VAS should be able to operate effectively as a sounder. VAS' nominal resolution (15 km at nadir view) will be roughly 20 km at the latitude of Oklahoma.

The NSSL radiosondes (launched every 90 minutes from sites roughly 50 km apart) were interpolated onto a 21 x 11 grid with approximately 20 km resolution using a Barnes objective analysis scheme (Barnes, *et. al.*, 1971). The gridded profiles serve as a "ground truth" for the sounding simulation experiment. Figure 3 is an SMS 11 micron image of the Texas-Oklahoma area at the time of the 2030 GMT 29 May 1976 frame listed in Table 4. The analysis grid is overlaid on Figure 3, showing a 200 x 400 km area encompassing the NSSL network. In order to simulate the coarser SFOV coverage (50 km) expected from VAS under operational conditions, a 7 x 5 subset of the 21 x 11 grid is used for clear air radiance simulations of all 10 NSSL frames. This 7 x 5 subgrid (50 km resolution) is the set of SFOVs actually used in the statistical and gradient studies in the following sections, while the original 21 x 11 grid (20 km resolution) is only used for image simulation. The SMS image in Figure 3 shows us that we can expect large enough cloud-free areas on either side of a developing instability for VAS to carry out soundings.

3.2 *Statistical Design*

The NSSL profiles and the corresponding simulated radiance fields are separated into two sets, dependent and independent, for establishing and testing the correlations between atmospheric

structure and VAS radiances. The first 6 of the 10 frames are used as the dependent training set, determining the clear air-to-radiance correlations needed for constructing the first guess and regression matrices used in this study. The remaining 4 of the 10 NSSL frames (drawn from just 2 NSSL events) are used as the independent test set for calculating the retrievability of atmospheric information from clear SFOV radiances. Since each frame contains 7 x 5 SFOVs, the NSSL6 training set has 210 dependent points, and the NSSL4 test set has 140 independent points, for retrieving temperature and moisture at 15 tropospheric levels. Both subsets have similar mean and covariance statistics.

The quality of profile retrievals is measured by the RMS residuals between the simulated VAS soundings and the "ground truth" profiles drawn from the NSSL analyses. The quality of gradient retrievals is judged from horizontal and vertical contour plots of analyzed soundings compared to the "ground truth" NSSL analyses. The usefulness of simulated VAS soundings for mesoscale analysis is demonstrated by the retrieval of a convectively unstable air mass.

The impact of progressively more detailed statistical conditioning is studied by comparing RMS profile residuals from retrievals conditioned with two other dependent sets: a "global" set supplied by NOAA from 32 widely distributed radiosondes and a wet/dry subset of the 6 "local" dependent NSSL frames. The NOAA32 are drawn from North American radiosonde/rocketsonde sites with a bias towards unusual profiles (Smith and Woolf, 1976). The "global" set is used here to establish statistics that are so broadly selected in time and space as to be unclassified. The NSSL wet/dry sets were selected by sub-classifying the individual NSSL6 profiles as "wet" or "dry," depending on whether the mixing ratio at 850 mb was more or less than 8 gm kg^{-1}, respectively.

4. VAS RADIANCE SIMULATION

In order to simulate a VAS frame over Oklahoma, radiances are computed from transmission functions for the temperature and moisture profile at each NSSL SFOV.

4.1 *Radiation Transfer*

The VAS radiance simulations use line-by-line transmission functions, $\tau(\nu, p)$, computed for each temperature, T(p), and mixing ratio, Q(p), profile. Radiances $R(\nu)$ in each channel, at nominal wavenumber ν, are computed by radiation transfer of the Planck function, $B(\nu, T)$, up from a perfectly emitting surface:

$$\tau(p) = \tau(\nu, p; T(p), Q(p); \text{lines, continuum}), \tag{1}$$

$$R = B(T(s))\,\tau(s) + \int_s^0 B(T(p))\,d\tau(p).$$

The U.S. Standard Atmosphere is used to fill in the stratopheric profile above the last reported radiosonde level. Topographic irregularities are accounted for by setting the 1000 mb and surface temperatures equal to the first reported radiosonde level, and surfaces are 100 percent emissive, giving isothermal bottomside structures with no radiance contrast. This assumption results in radiances that are correct for the actual topography, but it also results in a strong correlation between the lower troposphere and the surface, so that the lower tropospheric retrievals rely very heavily upon the window radiances.

Cloudy radiances are modeled with a simple cloud fraction n(x, y) at pressure level p', with cloud-top temperature T(c) equal to the air temperature T(p') for the SFOV:

$$R = [1 - n]\,[B(T(s))\,\tau(s) + \int_s^c B(T(p))\,d\tau(p)] \tag{2}$$

$$+ nB(T(c))\,\tau(c) + \int_c^0 B(T(p))\,d\tau(p).$$

4.2 *Simulated VAS Images*

Figure 3 shows the actual SMS 11 micron picture of the Texas-Oklahoma area taken at 2030 GMT 29 May 1976. In order to make realistic cloud height and coverage estimates, the cloud brightness temperatures T* (VISSR) are matched to a temperature profile estimate $T^0(p)$ of the scene, with iteration to produce a field of variable cloud fraction n(x, y) with the same cloud top

pressure p'. These cloud estimates are combined with the transmission functions for the analyzed SFOVs in the 21 x 11 grid to produce cloudy radiance fields, which are converted into VAS grey-level images with 20 km resolution. Some of these images are shown in Figures 4A, B and C where significant moisture gradients are visible through the openings in the clouds.

Figure 4 shows three simulated images of partly cloudy channels: the "VISSR window" (channel 8 at 11.2 microns), the "wet window" (channel 7 at 12.7 microns), and the difference in their brightness temperatures (T*(Ch8) - T*(Ch7)). The cloud tops appear as dark, cold SFOVs in the radiance images. In the cloudless areas, the brighter areas are warmer and dryer and the darker areas are cooler and wetter due to greater water vapor absorption. The appearance of this relative moisture gradient is enhanced by taking the difference between these "split window" channels. The differential image in Figure 4C has the brightest areas in the western portion of the NSSL frame where the two-channel differences are the greatest due to the absorption by the excess moisture there. The maximum contrast shown in Figure 4 is 5.5° K, which should dominate the expected single-sample noise (NEΔT = ±0.3° K in Table 1). Figures 11 and 12 show the actual cross sections of the temperature and moisture fields retrieved from this frame. These are discussed at length in section 6.

4.3 *Correlation Between Moisture and VAS Radiances*

The moisture gradient visible in the simulated VAS images suggests that we should look at the correlation between the VAS "split window" radiances and the moisture content of the lower troposphere. A clear correlation would be a basis for subdividing the local NSSL profiles into wet/dry subclasses for use in finely tuned dryline retrievals.

Figure 5 plots the brightness temperature differences (° K) between the "split window" channels against the mixing ratio (gm cm^{-3}) at 850 mb for the six dependent NSSL cases. There is the expected trend in the "split window" differences, with wetter SFOVs being darker due to the moisture blocking upwelling radiance more effectively at 12 microns. However, the scatter from frame to frame blurs the simple difference to moisture correlation enough to foil its use as

a direct predictor of absolute moisture content. A plot of total precipitable water (gm cm^{-2}) against the brightness difference (° K) in the "split window" produces roughly the same scatter as seen in Figure 5. The scatter in these simulated radiances is due entirely to natural variations in the temperature and moisture fields at other levels. Radiometric noise would contribute only another ±0.3° K to the brightness temperature differences. Correlation plots like Figure 5 understate VAS' net sensitivity to moisture, since each channel is influenced simultaneously by several atmospheric parameters. Retrieval algorithms combining all 12 VAS channels should be used to separate variables and to improve vertical resolution.

5. RESIDUAL ERRORS IN SIMULATED VAS SOUNDINGS

The conventional figure of merit (FOM) for profile retrievals is the RMS residual profile between the sounding and "ground truth." The "ground truth" in this study is simply the temperature and moisture profiles from which VAS radiances are simulated.

5.1 *Conditioned Regression Retrievals*

A minimum-information, linear regression algorithm is used to retrieve temperature and mixing ratio profiles from the simulated VAS radiances. This technique (Fleming and Smith, 1971) is chosen for the prelaunch demonstration of the VAS capabilities because it has enough flexibility to adjust both to VAS' programmable noise levels and to the statistical conditioning available in historical mesoscale radiosonde collections. Such statistical conditioning should improve retrievals by resolving ambiguities of vertical structure in favor of the most probable structure expected from objective experience (Chesters, 1980).

Regression retrievals assume that the radiance response $\delta R(\nu)$ in a channel at wavenumber ν, is a linear combination of atmospheric variations, $\delta X(p)$, where $X(p)$ is temperature, moisture, or other state parameter in the atmosphere as a function of pressure, p. Consequently, an estimate of the atmospheric variation, $\delta X'(p)$, can be made from a corresponding linear combination of variations in the observed radiances:

$$\delta R(\nu) = A(\nu, p) \cdot \delta X(p), \tag{3}$$

$$\delta X'(p) = C(p, \nu) \cdot \delta R(\nu).$$

The "$\cdot$" symbolizes matrix multiplication with terms being summed over matching independent variable values. With many observations of X and R, a retrieval matrix, $C(p, \nu)$, can be estimated from the radiance to atmosphere cross correlations in a set of observations:

$$C(p, \nu) = <\delta X(p)\, \delta R(\nu')> \cdot [<\delta R(\nu')\, \delta R(\nu)>]^{-1}. \tag{4}$$

The "$<...>$" symbolizes a statistical average over a sample learning set of simultaneous, colocated observations, and the "$[...]^{-1}$" symbolizes matrix inversion. The basis of the $<\delta X \delta R>$ correlation is the presence of T and Q within τ and B in equation 1. Likewise, the $<\delta R \delta R>$ channel-to-channel cross correlation is based both upon the underlying correlations within the state variables X and upon the overlap among the channels $d\tau/d\ln P$ (see Figures 1 and 2).

Direct application of the simple regression algorithm in equation 4 to a small set of available satellite and radiosonde data usually leads to retrieval matrices with large coefficients and opposing signs. This over-interprets the small fluctuations in real data. The minimum-information scheme conditions retrievals against this effect by incorporating an estimate of the radiometer noise in each channel $<\epsilon(\nu)^2>$.

Mathematically, the atmospheric variations and the corresponding radiance changes for a dependent set of events are linearized about the mean, and a single-sample noise, $\epsilon(\nu)$, is included:

$$X = <X> + \delta X,$$

$$R = <R> + \delta R + \epsilon,$$

$$\delta X' = C \cdot [\delta R + \epsilon],$$

$$d<[\delta X' - \delta X]^2>/dC = 0,$$

$$C = <\delta X \delta R> \cdot [<\delta R \delta R> + <\epsilon^2>]^{-1}$$

Equation 5 uses least squares techniques to solve for a matrix C (p, v), which minimizes the un-

certainty in the retrievals $\delta X'$ (p) averaged over a training set of dependent events. The radiometer noise can be expressed directly in radiance units (erg cm^{-2} sec^{-1} $wavenumber^{-1}$ $steradian^{-1}$, abbreviated "erg/etc."), or it can be computed from the single-channel variance $<\delta R\ (\nu)^2>$ divided by a corresponding "signal"/noise ratio $\gamma\ (\nu)$:

$$<\epsilon^2> = <\delta R^2>/\gamma^2 \qquad (6)$$

Note that the "signal" is the variance in the radiance, not the total brightness of a channel. The retrievals in this study are all done with a single "conditioning factor," $\gamma = 100/1$, which is optimistic for most of the VAS channels (see Table 2).

5.2 *"Local" vs. "Global" Retrieval Quality*

Simulated radiances for the clear SFOVs are used to determine the accuracy of temperature and moisture retrievals from soundings roughly 50 km apart. A "local" retrieval matrix is calculated using the six NSSL sets of 7 x 5 SFOVs by correlating the radiances with tropospheric temperatures and mixing ratios. For comparison, another retrieval matrix is calculated from the NOAA32 set of widely distributed radiosondes and their simulated radiances. Retrievals are done on the four independent NSSL test frames of 7 x 5 SFOVs with both the locally and widely conditioned matrices.

The RMS residuals in Figures 6 and 7 are the information not retrieved from these 140 clear, independent SFOVs because of vertical smoothing and noise conditioning. The NSSL retrievals are indeed much worse when they are made with matrices trained by statistics from a set of widely distributed radiosondes. The residual errors in the "globally" conditioned NOAA32 retrievals of the independent NSSL SFOVs are about ±4° C in temperature and ±25 percent in moisture, which are quite inaccurate for mesoscale weather analysis. The residual uncertainties in the "locally" conditioned NSSL6 retrievals are about ±1° C for the tropospheric temperature profile and ±25 percent for the mixing ratio profile, which are well within the VAS sounding requirements, although the moisture uncertainty is still too large to be useful for absolute mesoscale analysis. However, Figure 13, discussed in section 6, shows that local conditioning retrieves more

accurate relative moisture gradients, which are not discernible in these composite RMS profile statistics.

The moisture residuals are poorly determined in the lower troposphere, since VAS has only one moisture sensitive channel there, as indicated by the weighting functions in Figure 2. Neither the 100 mb nor the 1000 mb retrievals are meaningful, since the original NSSL radiosondes were rarely reported above 200 mb or below 920 mb. Profile uncertainties are dominated by mean residuals (not shown) over several unresolved vertical layers, as is normal with passive infrared sounding instruments. The temperature residuals are normally larger at the tropopause because there is little radiance from these cold, unresolved layers. Both the moisture and temperature residuals are normally greater near the surface because of the naturally greater atmospheric variability there.

Under real operating conditions, the uncertainty in the lower tropospheric profile will be even greater because of the unresolved clouds. The window channels will detect uneven emission from a surface that is less correlated with the "surface" air temperature than is assumed in this simulation. Operational temperature errors are expected to be about ±2° C; the temperature residuals in this study are only ±1° C because the radiances are simulated for optimal conditions.

5.3 *Fine Tuning the "Local" Retrieval Statistics*

The better quality of the "locally" conditioned soundings encouraged us to try even more detailed conditioning. "Dryline" conditioned retrievals are attempted by computing additional regression matrices from "wet" and "dry" subsets of the six dependent NSSL frames with SFOVs classified by whether the low level moisture, Q(850 mb), is more or less than 8 gm kg^{-1}. Retrievals are done upon selected SFOVs from the four independent NSSL test frames. The relatively bright (warm and dry) SFOVs in the 11 micron window are retrieved with the "dry" matrix, and the relatively dark (cool and moist) SFOVs are retrieved with the "wet" matrix. The RMS profile residuals from these wet/dry conditioned retrievals are plotted in Figures 8 and 9. For comparison, the original NSSL6 "locally" conditioned residuals are also plotted in these figures. The

wet/dry training scarcely improves the residuals, indicating that we have reached the point of diminishing returns by such detailed local conditioning.

5.4 *Retrieval of Vertically Integrated Parameters*

Since passive satellite radiances in each channel are accumulated over several hundred millibars of the troposphere (see Figures 1 and 2 and the third column of Table 2), one can expect satellite retrievals to represent vertically integrated parameters more accurately than single-level parameters. We examine the residuals in two integrated parameters derived from retrieved profiles for the four independent NSSL frames:

1. Precipitable water, measured in gm cm^{-2}, calculated by integrating the mixing ratio retrievals from 100 to 920 mb.
2. Geopotential thickness, measured in meters, calculated by integrating the temperature retrievals from 500 to 920 mb.

Table 5 lists both the mean and the standard deviation in the "ground truth" set and the residual errors for regression retrievals done with the "global" NOAA32 and with the "local" NSSL6 training sets. Note that the RMS error is the combination of the mean and standard deviation in the residuals and that a successful retrieval must have RMS errors less than the variance (standard deviation) in the "ground truth" set. Table 5 shows that:

1. The "ground truth" precipitable water in the four NSSL test frames is 2.49 ±0.39 gm cm^{-2}. The "global" NOAA32 retrievals did not improve the information about the precipitable water, since the RMS error (±0.39 gm kg^{-1}) is as large as the original variance. The "local" NSSL6 retrievals improved the uncertainty in the total precipitable water from ±0.39 to ±0.19 gm cm^{-2}, or only an 8 percent error in the total. The mean errors in the precipitable water retrievals are reasonably small for both retrieval matrices, which indicates that the "split window" (VAS channels 7 and 8) is working as planned.
2. The "ground truth" geopotential thickness in the four NSSL test frames is 4998 ±28.5 m. The NOAA32 "global" retrievals actually degraded the information about the thickness

field, with an RMS residual of ±31.2 m, due mostly to a mean underestimate of -30.5 m. The errors in the "globally" retrieved thickness field reflect the corresponding underestimates in the "globally" conditioned temperature profile retrievals discussed in the previous section. The NSSL6 "local" retrievals greatly improved the information about the thickness fields, leaving an RMS residual of only ±3.3 m.

In summary, the residual errors for the four independent NSSL test fields indicate that total precipitable water should be retrieved with less than ±25 percent error (even with poor statistical conditioning) and that geopotential thickness fields should be retrieved with "locally" conditioned methods in order to avoid serious mean errors. Analyzed fields of retrieved precipitable water and geopotential thickness will be examined in the following section.

6. MESOSCALE ANALYSIS OF VAS SIMULATED SOUNDINGS

An important objective of this VAS simulation experiment is to determine if VAS temperature and moisture retrievals can adequately delineate a convectively unstable air mass prior to the outbreak of severe convective storms. In order to demonstrate this, "ground truth" fields are compared to retrieved vertical cross sections, horizontal cross sections, and contour maps of vertically integrated parameters.

The 29 May 1976 case is selected for this part of the study, since this severe weather outbreak is an excellent example of a "dryline" propagating into Oklahoma. The lack of cloud cover over the NSSL network at the chosen time provided an opportunity for the realistic use of clear column radiances without cloud corrections, simulating optimal sounding conditions. The National Weather Service (NWS) surface analysis at 0000 GMT May 1976, shown in Figure 10, depicts a moderately strong low pressure system centered over the Texas panhandle. The most notable feature near the NSSL network is the dewpoint gradient due to the drier air moving eastward toward southwest Oklahoma. The SMS infrared image for 2030 GMT 29 May 1976 in Figure 3 shows a relatively clear region within the special network ahead of the developing convective storm cells in the Texas panhandle.

6.1 *Analysis of Horizontal Cross Sections*

The "ground truth" 850 mb temperature, mixing ratio, and equivalent potential temperature (θ_e) fields at 850 mb and 2030 GMT 29 May 1976 are shown in Figures 11A, D and G. This case lacks a significant temperature gradient across the network with only a 3° C range within the domain. On the other hand, there is a moisture maximum in western Oklahoma within which explosive convective development occurred by 0000 GMT 30 May 1976. The θ_e analysis reflects this moisture maximum and the resulting gradients across the central portion of the network.

Figure 11 also shows the 850 mb temperature, mixing ratio and θ_e analyses derived from the VAS simulated retrievals using the 7 x 5 SFOVs at 50 km resolution. Contour plots are shown for the two sets of retrievals, conditioned by the NOAA32 dataset and the NSSL6 dependent dataset. Comparison among the analyzed fields in Figure 11 reveals a general similarity in the main features with significantly different details:

1. The retrieved temperatures are within ±2° C of the "ground truth." However, the NOAA32 retrievals have a spurious temperature minimum in the center of the network, reversing the actual small east-west gradient in the western portion of the domain. The NSSL6 retrievals more accurately depict the structure of the warmer air, although the magnitude of the gradients is still weaker than the "ground truth."
2. The retrieved 850 mb mixing ratios are significantly underestimated by both sets of soundings shown in Figure 11. However, the NSSL-conditioned retrievals yielded mixing ratios 2 gm kg^{-1} higher than the NOAA32 retrievals in the region of maximum moisture and better accounted for the gradients of the moisture field, with the gradients in the central portion of the network nearly three times larger. There is a corresponding impact upon the gradients in the θ_e analyses.

In summary, Figure 11 shows that the "locally" conditioned retrievals do a better job of retrieving the horizontal structure in both temperature and moisture. The location and relative structure but not absolute magnitude, of the low level θ_e gradient are well retrieved.

6.2 *Analysis of Vertical Cross Sections*

Figure 12 shows corresponding vertical cross sections of temperature, mixing ratio and θ_e constructed from west to east through the middle of the network, intersecting the region of maximum moisture and convective instability (as measured by $d\theta_e/dz$). The cross sections of the "ground truth" data, in Figures 12A, D and G, again reveal the small temperature gradients and the maximum in moisture and θ_e in the western portion of the network. Of particular interest is the location of the strong vertical gradient of the mixing ratio just above the 850 mb level and the corresponding vertical gradient in θ_e. The large negative value of $d\theta_e/dz$ in the western portion of the domain illustrates that this region is indeed primed for the severe convective storms that developed there within the next 3 hours. Examination of the vertical cross sections of the NOAA32 and NSSL6 retrieval analyses reveals these interesting differences:

1. Both retrievals underestimate the moisture content and the vertical gradients. The NOAA32 cross section in Figure 12E actually has a larger moisture value in the lower troposphere, but shows a more gradual vertical gradient than the NSSL6 cross section in Figure 12F. However, the NSSL6 moisture retrievals better depict the magnitude and location of the vertical moisture gradient. This behavior can be related to the makeup of the moisture profiles in the NOAA32 and NSSL6 training datasets. The lower tropospheric moisture information embodied in the NOAA32 is determined by tropical profiles, which have a large concentration of moisture in the boundary layer and a gradual decrease with height. The moisture information in the NSSL dataset is basically drier, but typical profiles have a sharp gradient near the 850 mb level. Consequently, these pre-thunderstorm structures are only approximately reproduced by the corresponding retrieval matrices, because the broad weighting functions shown in Figures 1 and 2 are unable to resolve the vertical structure of the moisture in the lower troposphere.
2. Both retrieval sets in Figure 12 underestimate θ_e in the lower troposphere due to the deficiencies in the moisture retrievals. Yet, both retrievals do in fact capture a region of

maximum θ_e and $d\theta_e/dz$ in the region of maximum convective instability. The NSSL6 retrievals locate the maximum $d\theta_e/dz$ gradient more accurately at the critical 850 mb level than do the NOAA32 retrievals. Thus, the "locally" retrieved θ_e field is more representative of the actual convective instability shown in Figure 12G.

3. The lifted index (LI), which is a measure of the atmospheric instability, is computed for the most unstable region of the NSSL network, as determined by the θ_e cross sections in Figure 12G. The LI is -10 for the "ground truth" data, indicating a very unstable environment conducive to the development of severe convective storms. For both the "global" NOAA32 retrievals and the "local" NSSL6 retrievals, the LI is -4. Thus, the simulated VAS retrievals capture a potential instability, although its magnitude is reduced.

In summary, Figure 12 shows that the "local" conditioning does a better job of estimating the vertical moisture structure. The potentially unstable air mass is well located in the retrievals, but its magnitude is underestimated due to the lack of vertical resolution in the VAS channels and to the lack of ancillary surface data in this simulation.

6.3 *Analysis of Integrated Parameters*

The RMS statistics for precipitable water and geopotential thickness retrievals over all four independent NSSL test sets indicate that these integrated parameters should be a better measure of satellite sounding quality than single-level cross sections. To demonstrate this point for an analyzed field, contour maps of total water and thickness are produced from the retrievals for the 2030 GMT 29 May 1976 frame. Figures 13A, B and C show precipitable water (100 to 920 mb), and Figures 13D, E and F show geopotential thickness (500 to 920 mb). Comparison of the "ground truth" fields to the "global" NOAA32 retrievals and the "local" NSSL6 retrievals confirms the trends seen in the 850 mb level cross sections in Figure 11:

1. The "ground truth" precipitable water field in Figure 13A has a strong gradient from east to west (ranging from 1.47 to 3.25 gm cm^{-2} with a mean and standard deviation of 2.27 $\pm$0.46 gm cm^{-2}). The precipitable water is somewhat underestimated with both

retrievals, although the residual error is small (averaging +0.09 ±0.37 gm cm^{-2} for the "global" field, and only -0.03 ±0.12 gm cm^{-2} for the "local" field). The location and gradients in the total water are roughly captured in both retrievals, but with noticeably better detail in the "local" retrievals. Apparently, the "split window" channels can deliver enough unambiguous information about the total water content to avoid serious retrieval errors even with poor statistical conditioning.

2. The "ground truth" geopotential thickness field in Figure 13D has only weak gradients from east to the southwest corner (ranging from 5018 to 5048 m with a mean and standard deviation of 5029 ±5.2 m). The small variance reflects the weak underlying temperature gradients. The "globally" conditioned thickness retrieval field in Figure 13E is a very poor representation of the "ground truth": the weak eastern minimum is exaggerated, the spurious warm retrievals in the center produce a spurious maximum, the gradient in the southwest corner is missed, and all thickness values are much too low (averaging -33.5 ±5.9 m). Apparently, the radiance signature in the moisture channels is being incorrectly interpreted as tropospheric temperature variations by the "global" regression statistics, since Figure 13E looks like a combination of the moisture and temperature features seen in both Figures 13A and D. The "locally" conditioned thickness field in Figure 13F is in much better agreement with the "ground truth" field, with most of the error in the form of a small overestimate for the entire "locally" retrieved field (averaging only +4.0 ±2.8 m).

In summary, Figure 13 shows that analyzed fields of parameters integrated over the simulated VAS retrievals are estimated well enough to distinguish outstanding mesoscale features, especially when the retrievals are "locally" conditioned. Residuals are dominated by mean errors in the absolute strength of the field. Therefore, VAS can be expected to be a very good instrument when used for capturing relative horizontal gradients within a mesoscale field.

7. SUMMARY AND DISCUSSION

The VISSR Atmospheric Sounder (VAS) is designed to operate as an integral part of the GOES system, providing an interactive sounding capability from geosynchronous orbit for the first time. VAS has 12 calibrated thermal infrared channels in the CO_2 and H_2O molecular bands between 4 and 15 microns. The channels are chosen to distinguish the effects of tropospheric temperature, moisture and cloud cover upon the upwelling radiances. The geosynchronous nature of VAS is a key element for the observation of the development of mesoscale weather systems, typically surveying the United States in all 12 bands once per hour with 15 km (nadir view) resolution. Satellite soundings derived from such multispectral scenes will have 30 to 60 km effective resolution, since several pixels will have to be averaged to reduce radiometric noise and to deal with broken cloud cover in the net sounding field of view.

This report describes a prelaunch sounding simulation experiment to demonstrate:

1. The visibility of lower tropospheric moisture gradients in the VAS radiances.
2. The detectability of a potential convective instability in a pre-thunderstorm environment, using optimal soundings from the VAS channels.
3. The sensitivity of residual errors in VAS regression retrievals to "local" statistical conditioning for the kind of mesoscale phenomenon under investigation.

In order to estimate the accura of the three-dimensional VAS soundings within severe local storm systems, 12-channel radiance fields are simulated for thunderstorm environments observed in Oklahoma. Temperature and moisture profiles for 10 time frames are drawn from the radiosonde network operated by the NSSL in 1976. The profiles are gridded using a Barnes analysis, covering Oklahoma with a grid at 20 km horizontal resolution and the troposphere at 1 km vertical resolution. Radiances are simulated for SFOVs in each frame, using line-by-line transmission functions for the temperature and moisture profiles.

Simulated VAS images of partly cloudy pre-storm conditions are shown for one of the NSSL frames where a corresponding SMS 11 micron picture is available. Radiances are computed at

full VAS resolution (20 km projected view per SFOV). Grey level images in the "split window" channels at 11 and 12 microns show that realistic cloud cover does not seriously mask the underlying precursor storm conditions. Moisture gradients are visible in the clear areas with contrast greater than the expected VAS noise levels.

Temperature and moisture profile retrievals are done at the expected SFOV resolution by using a coarser (50 km) SFOV subset drawn from the finer (20 km) grid. These simulated radiances are separated into two sets: a "local" dependent training set used to determine clear air-to-radiance correlations and an independent test set used to determine the retrievability of atmospheric information from clear SFOVs. The impact of detailed statistical conditioning upon a regression retrieval scheme is demonstrated by comparing these "locally" conditioned retrievals to soundings done with two other dependent training sets: a "global" set derived from 32 North American radiosondes and a wet/dry subset of the "local" dependent NSSL frames. For the latter comparison, the fields are partitioned into a "wet set" and a "dry set," using a threshold mixing ratio of 8 gm kg^{-1} at 850 mb.

Results from the simulated retrievals include:

1. Temperature profile residual errors in the troposphere are ±2° C across a 3° C gradient, and corresponding mixing ratio residuals are ±2 gm kg^{-1} across an 8 gm kg^{-1} gradient.
2. Horizontal and vertical temperature and moisture structures are retrieved in the lower troposphere, and potentially unstable air is recovered from simulated VAS radiances having the resolution and noise limits expected from the instrument. The absolute magnitude of the retrieved potential instability is significantly underestimated by the remote sounding process, which reflects the lack of vertical resolution in the 12 VAS channels. Relative temperature and moisture patterns are retrieved, although the magnitudes of the gradients are likewise underestimated.
3. Retrievals done with regression matrices conditioned with "local" weather statistics have smaller residual errors than those conditioned with "global" data. These results are due

to the better resolution of ambiguities in vertical structure in favor of the most probable structure derived from a "local" statistical database. A further subdivision of the dependent NSSL6 dataset into "wet" and "dry" subsets did not make any statistically significant improvement in the "local" retrievals.

4. VAS should be capable of retrieving vertically integrated meteorological parameters. The main moisture and airmass features are captured in the form of retrieved fields of precipitable water and geopotential thickness. These simulations had only ±0.2 gm cm^{-2} error (less than 25 percent) in precipitable water and only ±3.3 m error in the 500 to 920 mb thickness, using "locally" conditioned regression coefficients. The inadequacies of the "globally" conditioned retrievals are most dramatically displayed in retrieved thickness fields.

This prelaunch study of VAS retrievability gives promising results for pre-thunderstorm environments. Profile errors are comparable to those claimed for polar orbiting sounding instruments. Strong gradients are discernible in realistic partly cloudy conditions, although their magnitudes are underestimated like those observed with operational sounders. While not all of the complex factors in satellite data have been simulated in this study (such as multiple cloud structures, surface irregularities, reflected sunlight, and radiometric errors), these results still imply that VAS radiances will produce the best sounding when a human being classifies the scene, picks relatively clear areas for retrieval, and applies a "local" statistical database. The VAS simulated soundings show the same limitations in absolute accuracy and vertical resolution that are suffered by other passive infrared satellite instruments, especially in the lower tropospheric moisture retrievals. This weakness, even in these optimally simulated soundings, indicates that timely incorporation of conventional surface data will have to become part of VAS data processing to make the lower tropospheric retrievals more accurate. Nevertheless, VAS' spatial and temporal resolution should permit us to locate and effectively monitor the relative changes within potentially unstable mesoscale structures, and thus significantly improve upon the synoptic scale, ground-based and polar

orbiting data networks. The analysis of real VAS data will determine if this potential for monitoring mesoscale atmospheric changes can be realized with geosynchronous satellite sounding data.

ACKNOWLEDGEMENTS

This work is funded through the VAS Demonstration project of NASA's Operational Satellite Improvement Program (OSIP) and is managed by Dr. Harry Montgomery of NASA/GSFC. The effort to simulate prelaunch VAS soundings of severe storm conditions was initiated by Dr. Albert Arking of NASA/GSFC, who also made several useful suggestions for improving the manuscript. We thank Mr. Wayne Robinson, Mr. Wally Gross and Dr. Tay-How Lee of Computer Sciences Corporation for their work in carefully preparing many of the datasets for our use.

REFERENCES

1. Barnes, S. L., J. H. Henderson, and R. J. Ketchum, *Rawinsonde Observation and Processing Techniques at the National Severe Storms Laboratory*, National Oceanic and Atmospheric Administration, Technical Memorandum ERL NSSL-53 (available as NTIS-72N 12551), 1971.
2. Burch, D. E., D. A. Gryvnak, and J. D. Pembrook, *Investigation of the Absorption of Infrared Radiation by Atmospheric Gases*, AFCRL-70-0373 (available as NTIS-70N42640), 1970.
3. Burch, D. E., D. A. Gryvnak, and J. D. Pembrook, *Investigation of the Absorption of Infrared Radiation by Atmospheric Gases: Water, Nitrogen, Nitrous Oxide*, AFCRL-71-0124 (available as NTIS-71-X78131), 1971.
4. Chesters, D., "Statistically Conditioned Least-Squares Retrievals Planned for the VAS Demonstration Experiment," *VAS Demonstration Workshop*, ed., D. L. Endres and L. W. Uccellini, NASA Conference Publication 2157, 67-79 (available as NTIS-81N 19709), 1980.
5. Fleming, H. E., and W. L. Smith, "Inversion Techniques for Remote Sensing of Atmospheric Temperature Profiles." *Fifth Symposium on Temperature* (Washington, D.C.) (available as NTIS-73A 41976), 1971.
6. Hayden, C. M., "Low Level Moisture from VAS," *VAS Demonstration Workshop*, ed., D. L. Endres and L. W. Uccellini, NASA Conference Publication 2157, 57-65 (available as NTIS-81N 19709), 1980.
7. Hillger, D. W., and T. H. Vonder Haar, "Deriving Mesoscale Temperature and Moisture Fields from Satellite Radiance Measurements over the United States," *J. Appl. Meteor., 16*, 715-726, 1977.
8. Hillger, D. W., and T. H. Vonder Haar, "An analysis of Satellite Infrared Soundings at the Mesoscale Using Statistical Structure and Correlation Functions," *J. Atmos. Sci, 36*, 287-305, 1979.
9. McClatchey, R. A., W. S. Benedict, S. A. Clough, D. E. Burch, R. F. Calfee, K. Fox, L. S.

Rothman, and J. S. Garing, *AFCRL Atmospheric Absorption Line Parameter Compilation, AFCRL-TR-73-0096* (available as NTIS-73N 30382), 1973.

10. Mostek, A., L. W. Uccellini and W. Gross, *A Description of the NSSL Cases Used for a Simulated VAS Retrieval Study, NASA TM 80223* (available as NTIS-81NO 12678), 1980.
11. Phillips, N., L. M. McMillin, A. Gruber, and D. W. Wark, "An Evaluation of Early Operational Temperature Soundings From TIROS-N," *Bull. Amer. Meteor. Soc., 16,* 1158-1197, 1979.
12. Prabhàkara, C., G. Dalu, and V. G. Kunde, "Estimation of Sea Surface Temperature from Remote Sensing in the 11 to 13 Micron Window Region," *J. Geophys. Res., 79,* 5039-5044, 1974.
13. Roberts, R. E., J. E. A. Selby, and L. M. Biberman, "Infrared Continuum Absorption by Atmospheric Water Vapor in the 8-12 Micron Window," *Applied Optics, 15,* 2085-2090, 1976.
14. Schlatter, T. W., "An Assessment of Operational TIROS-N Temperature Retrievals over the United States," *Mon. Wea. Rev., 109,* 110-119, 1981.
15. Smith, W. L. and H. M. Woolf, "The Use of Eigenvectors of Statistical Covariance Matrices for Interpreting Satellite Sounding Radiometer Observations," *J. Atmos Sci., 33,* 1127-1140, 1976.
16. Smith, W. L., C. M. Hayden, H. M. Woolf, H. B. Howell, and F. W. Nagel, "Interactive Processing of TIROS-N Sounding Data." *Conference on Weather Forecasting, Analysis and Aviation Meterology* (Silver Spring, MD) AMS, Boston, 390-395 (available as NTIS-79A 31851), 1978.

TABLE 1

Prelaunch specifications for the 12 VAS channels, all of which have 15 km (nadir view) resolution.

VAS CH #	FILT CENT μ	FILT CENT cm^{-1}	FILT BAND cm^{-1}	PURPOSE FOR SOUNDING	MAIN ABS GAS	OTHER SIGNIF EFFECTS	SAMPLE NOISE $\pm^{\circ}$ K	SFOV REQ $\pm^{\circ}$ K	NOMINAL SPIN BUDGET
1	14.7	678	10	temp	CO_2	O_3	5.3	.3	38
2	14.5	691	16	temp	CO_2	O_3	2.2	.3	10
3	14.3	699	16	temp	CO_2	O_3	1.8	.3	7
4*	14.0	713	20	temp	CO_2	O_3	1.2	.2	4
5*	13.3	750	20	temp	CO_2	H_2O	1.0	.2	4
6	4.5	2209	45	temp+cloud	N_2O	sun	1.6	.1	35
7*	12.7	787	20	moisture	H_2O	CO_2	1.0	.2	4
8*	11.2	892	140	surface		H_2O+CO_2	0.1	.2	1
9*	7.3	1370	40	moisture	H_2O		3.4	.4	25
10*	6.8	1467	150	moisture	H_2O		1.6	.5	2
11	4.4	2254	40	temp+cloud	CO_2	sun	6.7	.3	46
12	3.9	2540	140	surface		sun+H_2O	0.8	.1	4

*Available at 7 km (nadir view) resolution.

TABLE 2

Estimated sensitivity of the VAS channels for nadir view simulations of the U.S. Standard Atmosphere and a set of 32 "globally" distributed radiosondes.

VAS CH #	PEAK WEIGHT (mb)	10%-90% RADIANCE LAYER (mb)	NET SENSITIVITY (°K/ °C) TEMP	DEWPT	SURF	EARTH MEAN (°K)	EARTH σ (±°K)	"SIGNAL" /NOISE (°K/°K)
1	70	4-120	1.00	-.00	.00	219	10	2
2	125	4-225	.99	-.00	.00	219	9	4
3	200	15-475	.91	-.02	.00	223	7	4
4	500	40-900	.73	-.09	.02	238	9	7
5	920	420-surf	.47	-.30	.29	260	15	15
6	850	520-surf	.43	-.03	.44	257	17	11
7	1000	720-surf	.33	-.37	.63	270	19	19
8	surf	920-surf	.17	-.20	.84	272	21	210
9	600	110-820	.82	-.70	.02	254	10	3
10	400	240-620	.94	-.70	.00	246	7	4
11	300	7-1000	.80	-.01	.04	237	11	2
12	surf	surf-surf	.08	-.03	.92	273	22	27

TABLE 3

The NSSL6 datasets used to "locally" condition regression matrices for simulated VAS soundings.

FRAME	TIME	DATE	DESCRIPTION OF 6 NSSL EVENTS
1	2030 GMT	12 May 1976	A strong east-west squall line, associated with cyclogenesis in the Texas panhandle, moved to the south through the network.
2	2030 GMT	21 May 1976	Scattered storm cells near the northwest corner of the network were associated with a stalled leeside trough west of Oklahoma.
3	1900 GMT	26 May 1976	Areas of scattered activity developed over the network near the warm and cold fronts associated with a low pressure system that moved over the area from the Texas panhandle.
4	1900 GMT	12 June 1976	A few cells appeared in the northwest corner of the network just ahead of a slowly propagating dryline.
5	2330 GMT	14 June 1976	A strong storm developed in response to a short wave propagating southeast over the network, initiated by the intersection of a frontal boundary with a pre-existing dryline.
6	0100 GMT	18 June 1976	Strong storms developed in response to frontal and dryline interaction, as a weak short wave propagated eastward through the network.

TABLE 4

The NSSL4 datasets used to test simulated VAS soundings. The four frames are drawn from the initial and developing stages of two well observed storms. The frame at 2030 GMT 29 May 1976 is used to simulate VAS images.

FRAME	TIME		DATE	DESCRIPTION OF 2 NSSL EVENTS (4 frames)
7	2330	GMT	22 May 1976	A strong upper level wave broke down a block-
8	0100	GMT	23 May 1976	ing ridge and inversion to induce dynamics that resulted in a dryline frontal passage. A strong squall line developed along a moist tongue ahead of the front.
9*	2030	GMT	29 May 1976	An upper level long wave over the Rocky Moun-
10	2330	GMT	29 May 1976	tains supported cyclogenesis in the Texas-Okla- homa panhandles. A weak cold front combined with a wedge of hot, dry air behind a dryline and rapid moisture inflow from Gulf of Mexico, providing a classic example of rapid convective development directly over the NSSL network.

*Cloud cover estimate is available from SMS 11 micron image.

TABLE 5

Mean and standard deviations of precipitable water and geopotential thickness from the NSSL4 test set for the "ground truth" profiles and residual errors in the "global" and "local" retrievals.

CASE	PRECIPITABLE WATER (gm cm^{-2}, 100-920 mb)	GEOPOTENTIAL THICKNESS (meters, 500-920 mb)
"Ground Truth"	2.49 ± 0.39	4998. ± 28.5
"Global" Residuals	-0.01 ± 0.39	-30.5 ± 6.9
"Local" Residuals	-0.10 ± 0.16	+ 2.1 ± 2.5

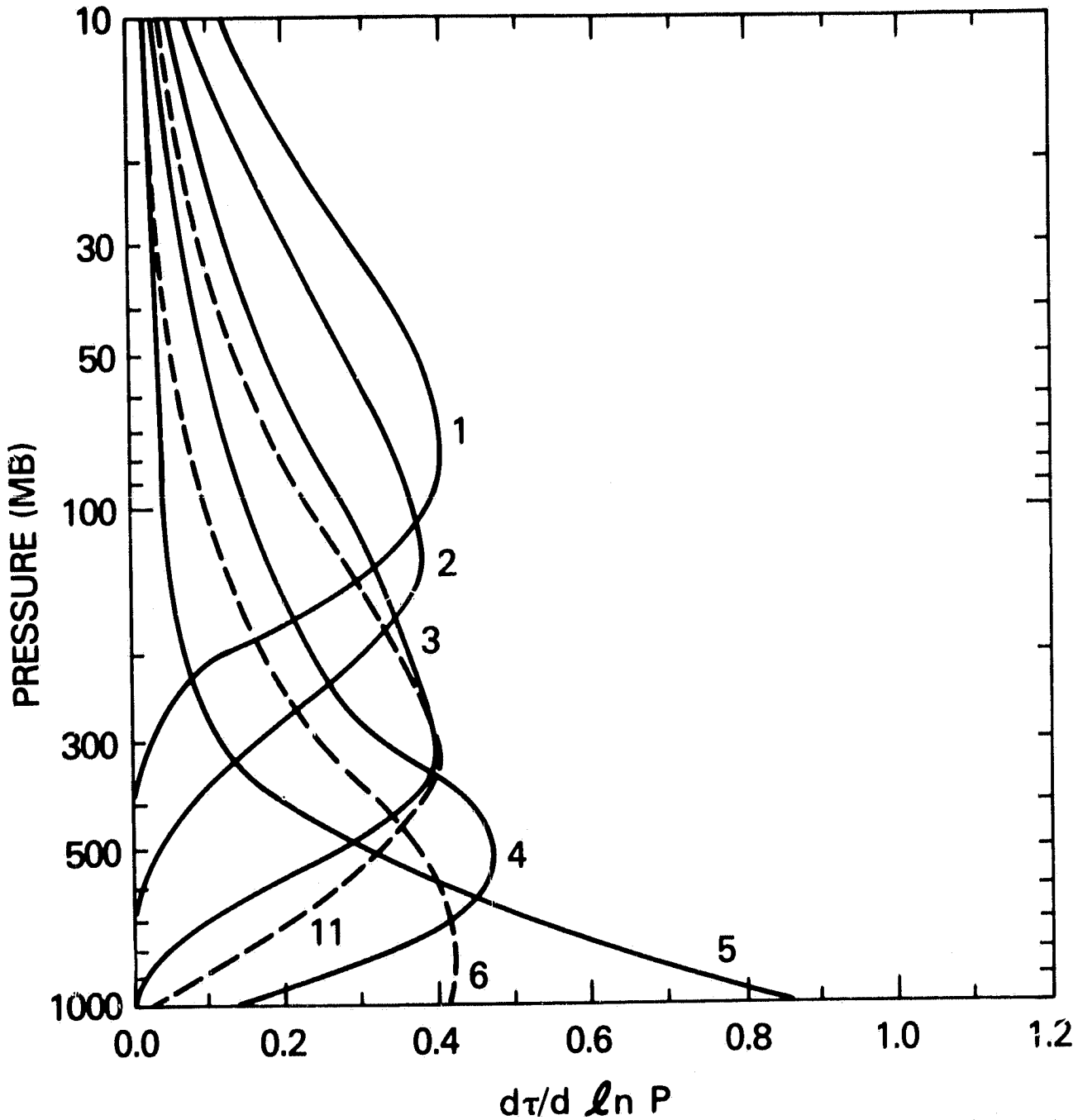

Figure 1. VAS weighting functions for the seven temperature sounding channels.

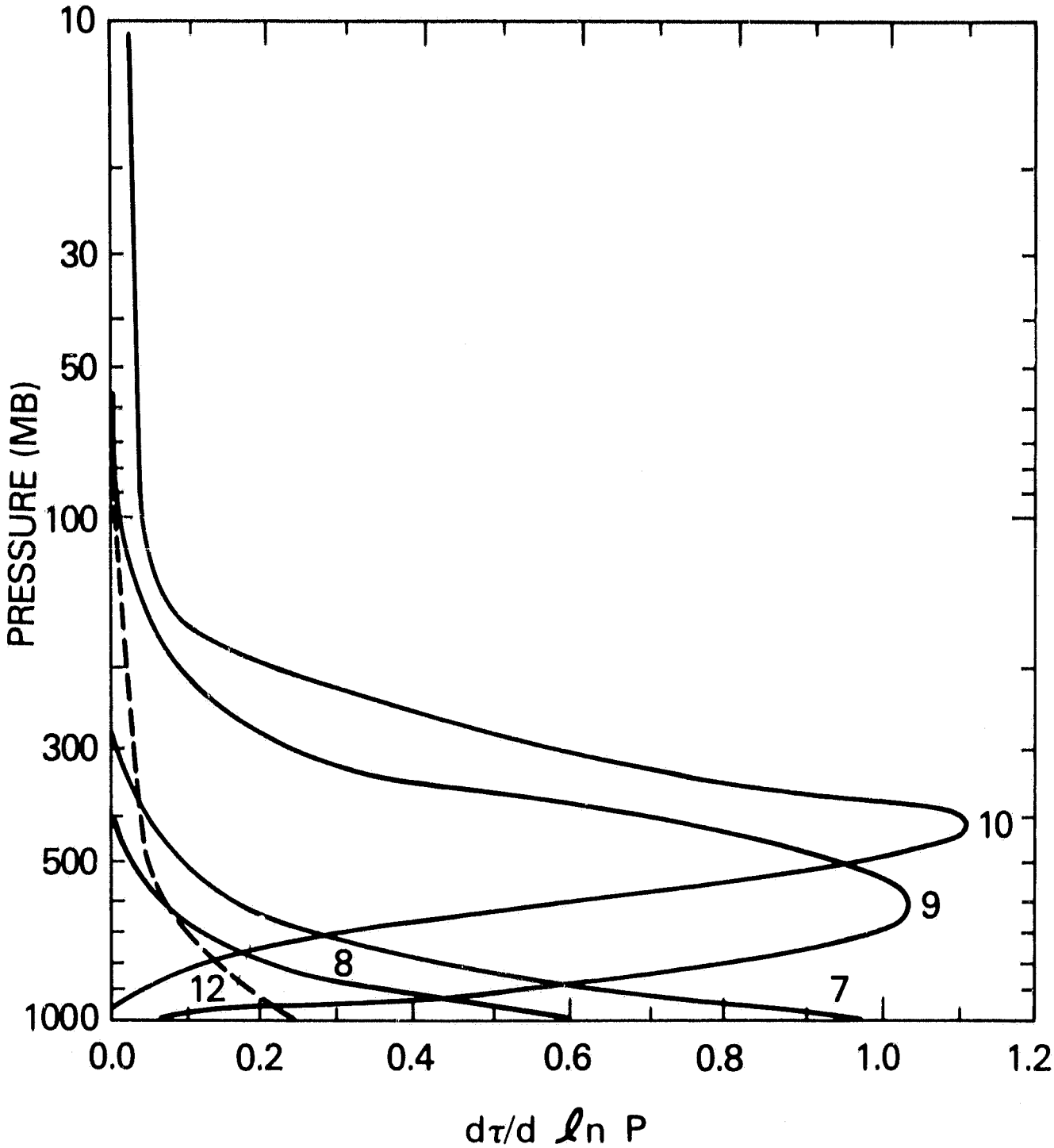

Figure 2. VAS weighting functions for the three moisture sounding and two window channels.

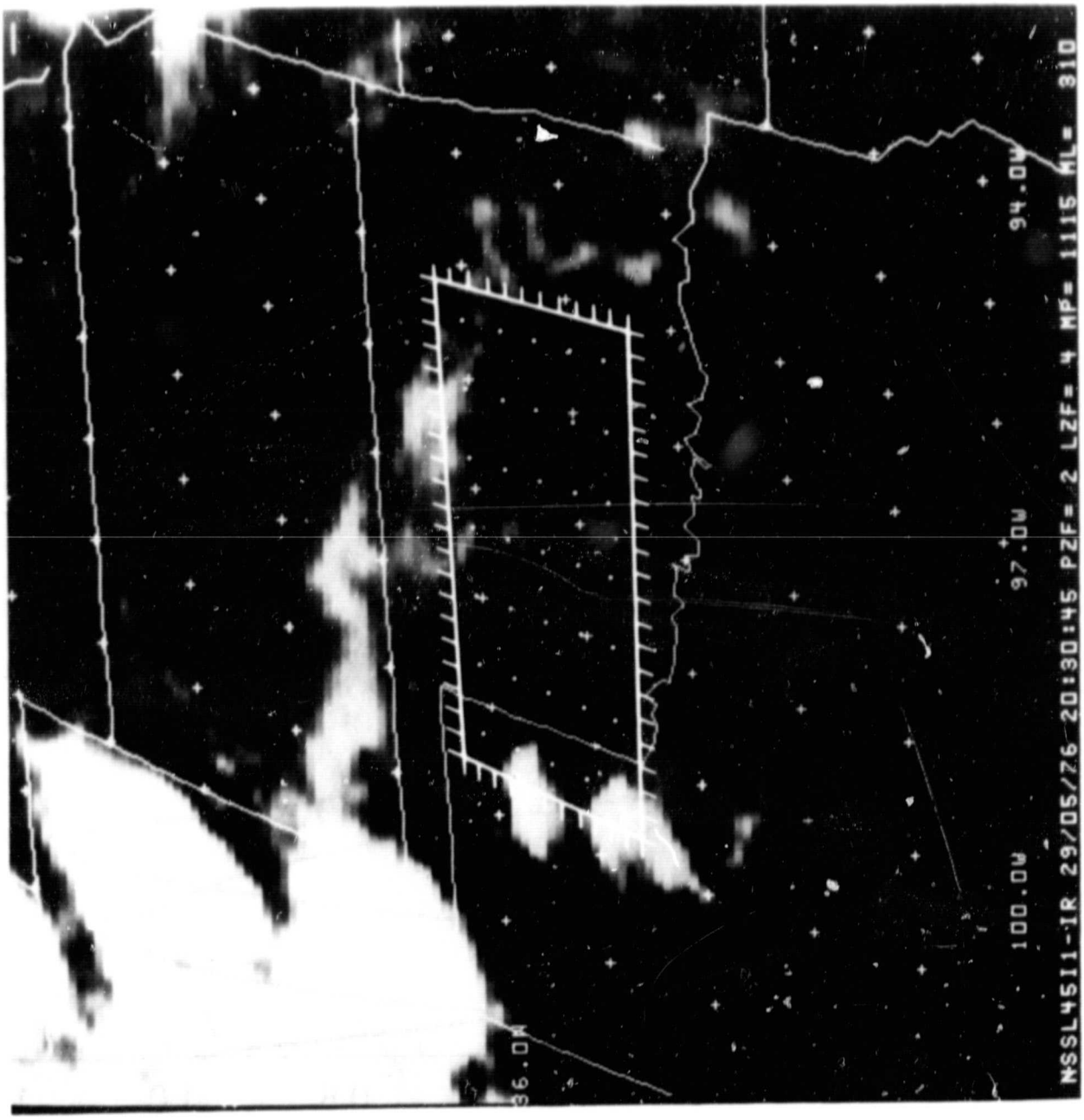

Figure 3. SMS 11 micron image on 29 May 1976 at 2030 GMT with an overlay of the 21 x 11 Barnes analysis grid at 20 km resolution for simulated VAS images and an imbedded 7 x 5 grid at 50 km resolution for simulated soundings.

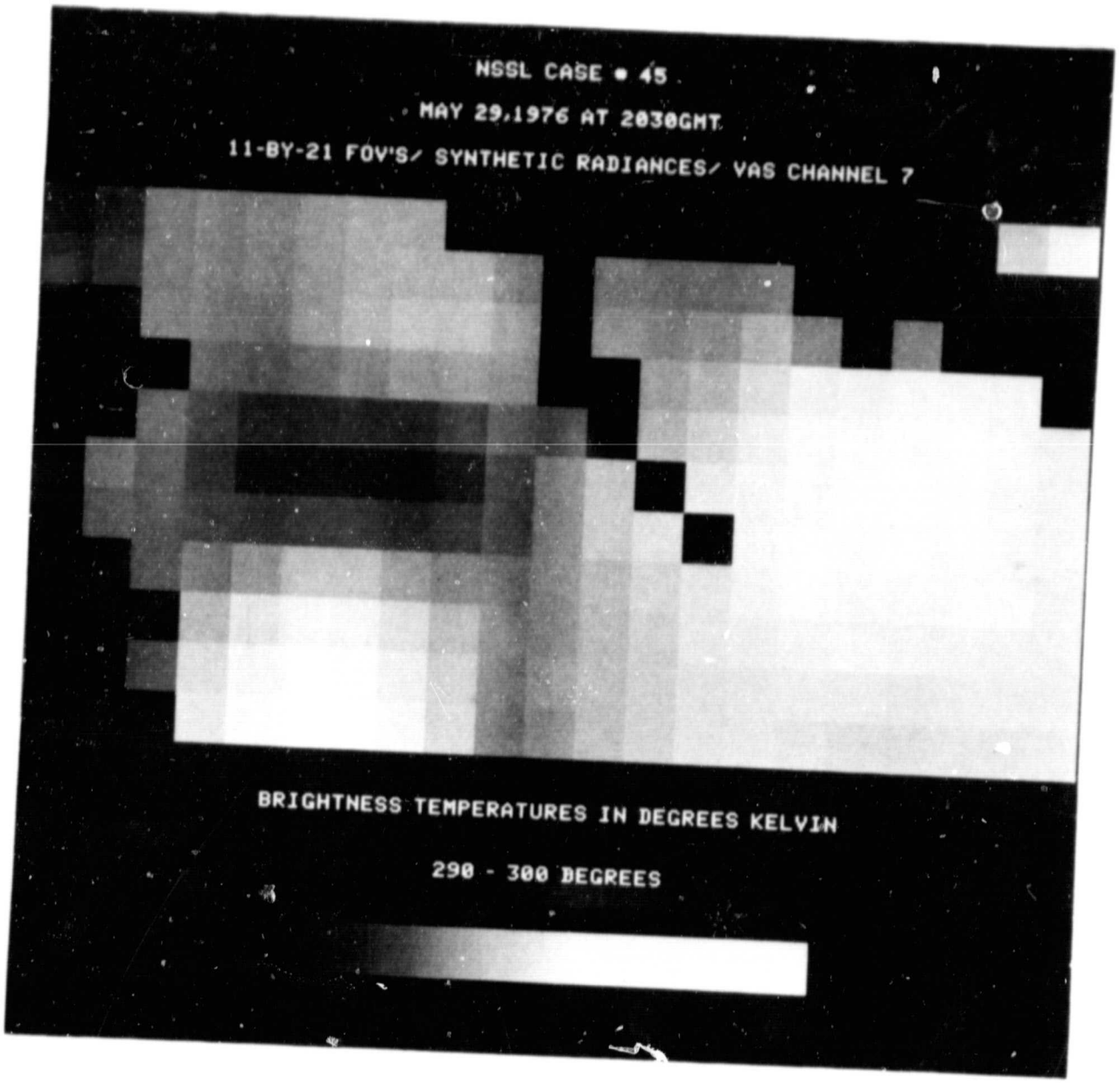

Figure 4a. Synthetic VAS brightness temperature images for a pre-storm environment at 2030 GMT 29 May 1976, using the 20 km analysis grid and SMS cloud estimates.

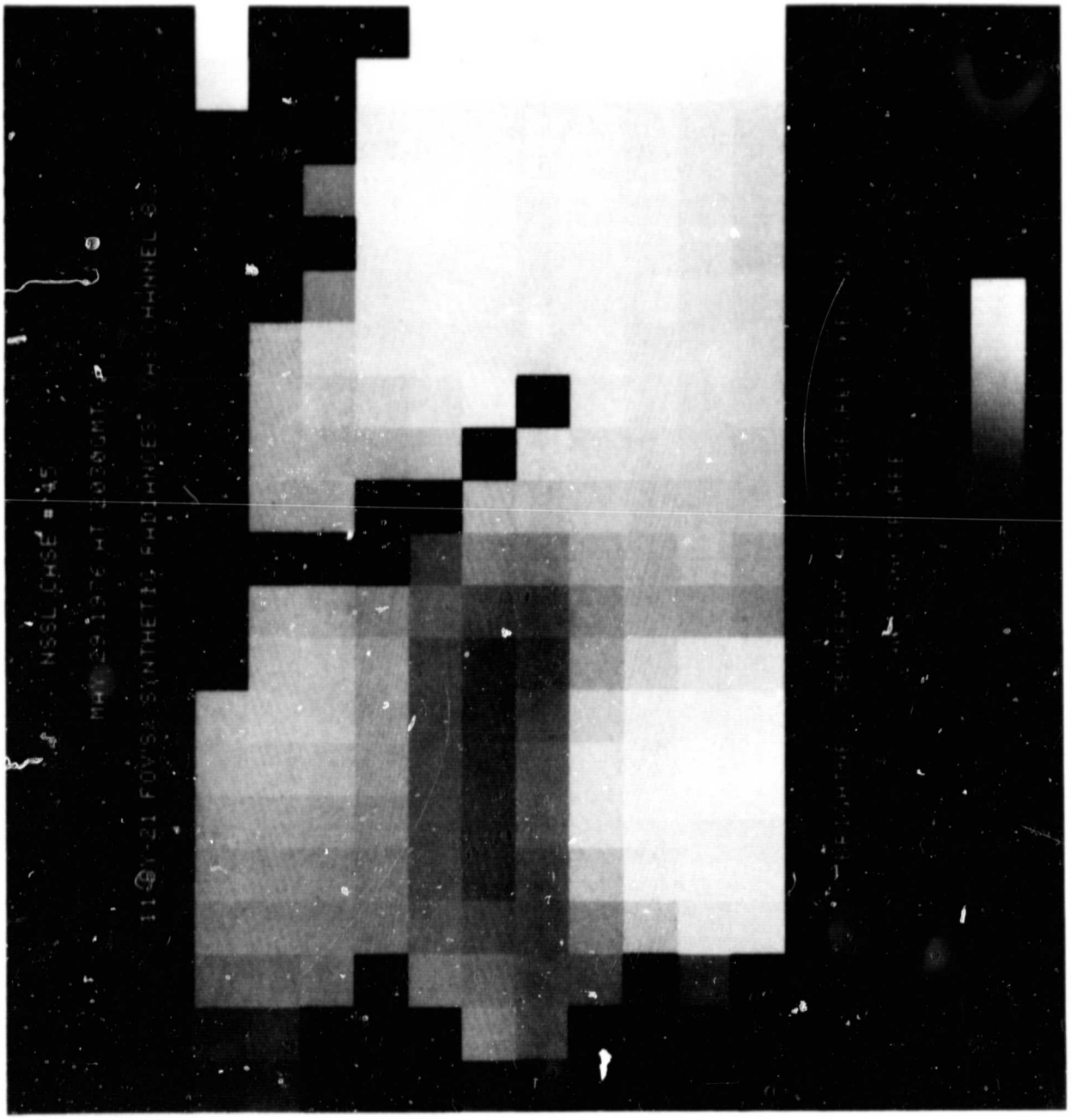

Figure 4b. Synthetic VAS brightness temperature images for a pre-storm environment at 2030 GMT 29 May 1976, using the 20 km analysis grid and SMS cloud estimates.

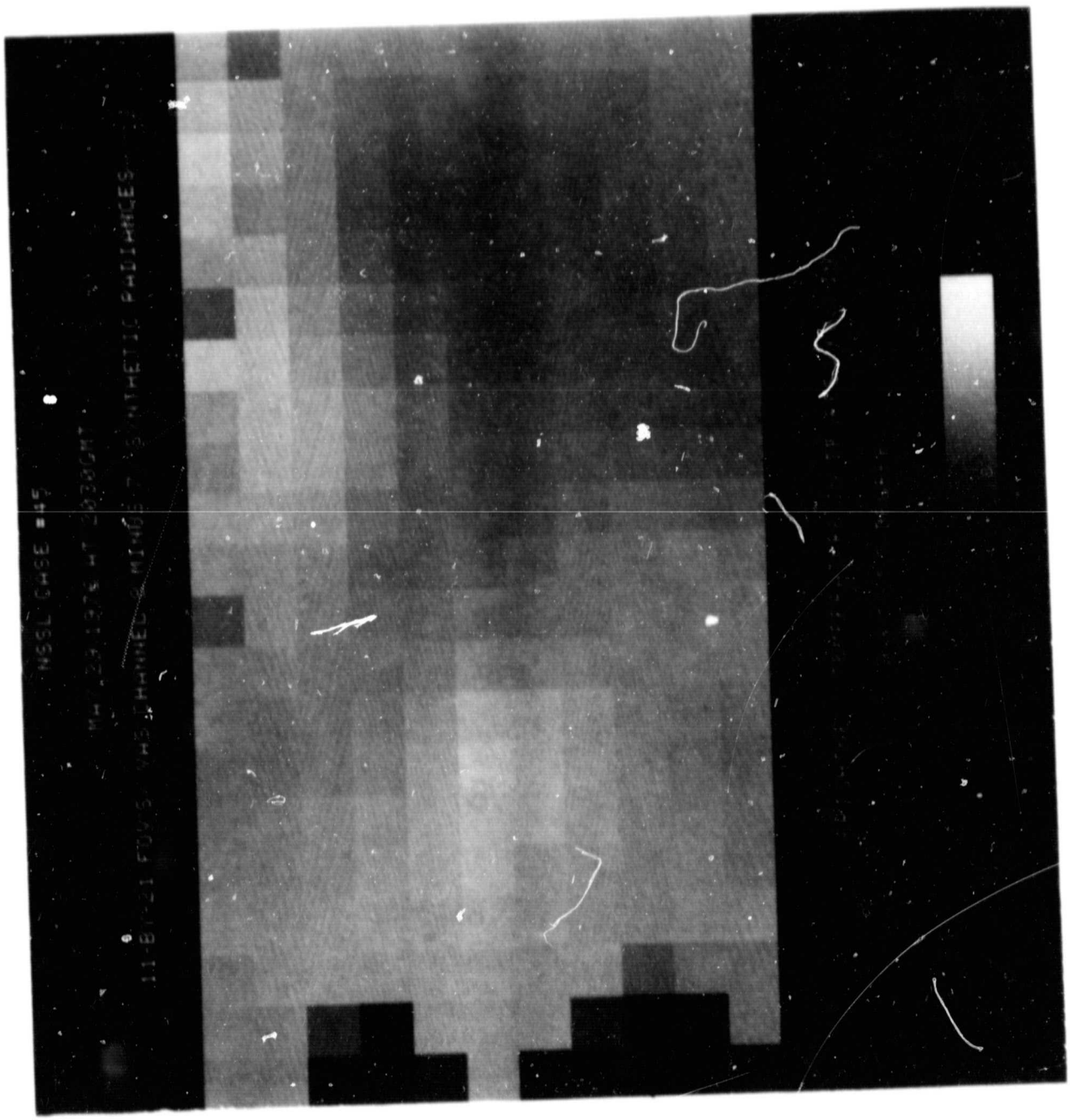

Figure 4c. Synthetic VAS brightness temperature images for a pre-storm environment at 2030 GMT 29 May 1976, using the 20 km analysis grid and SMS cloud estimates.

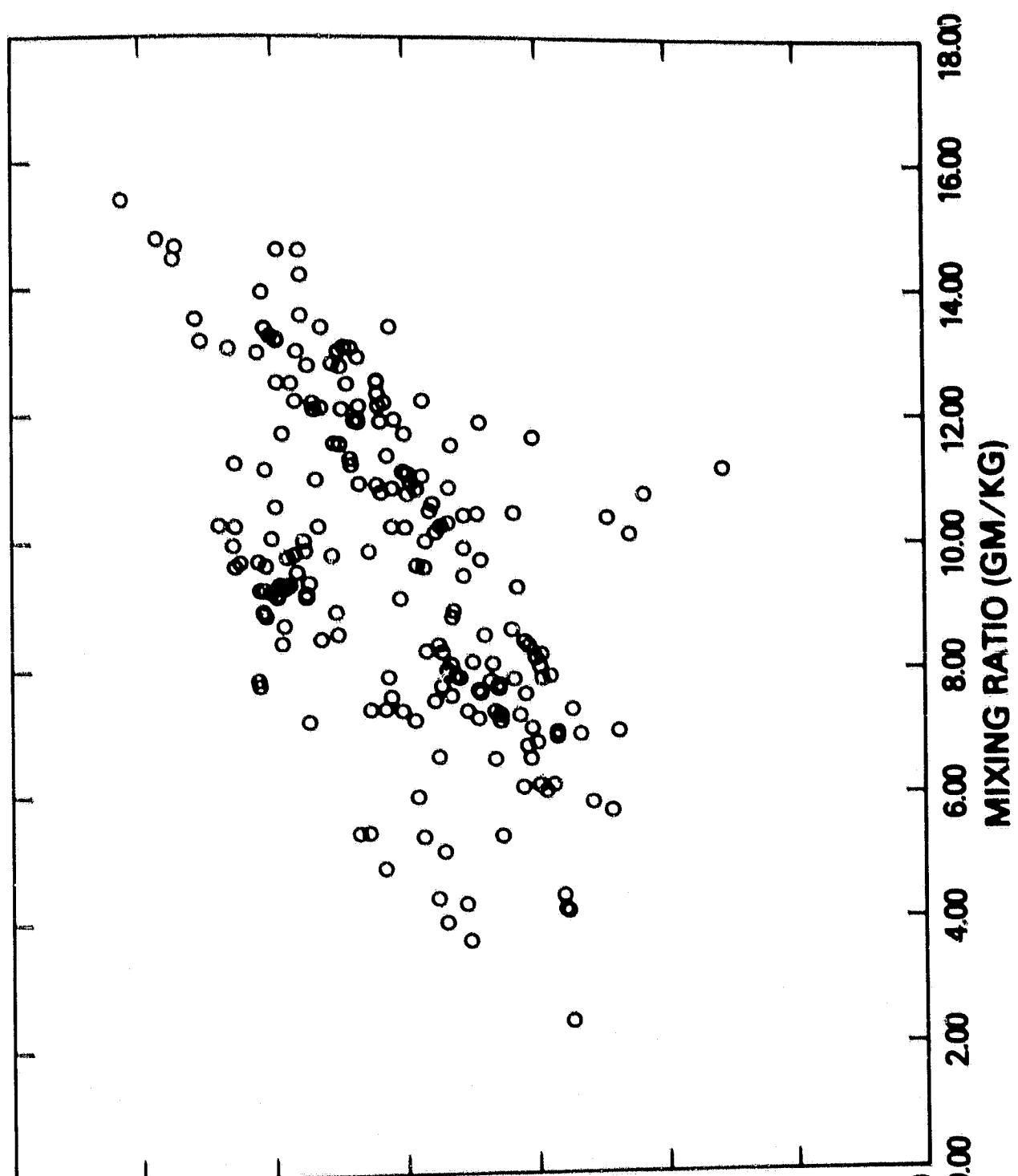

Figure 5. "Split window" brightness temperature differences plotted against the corresponding low level moisture for all 210 SFOVs in the NSSL6 dependent training frames.

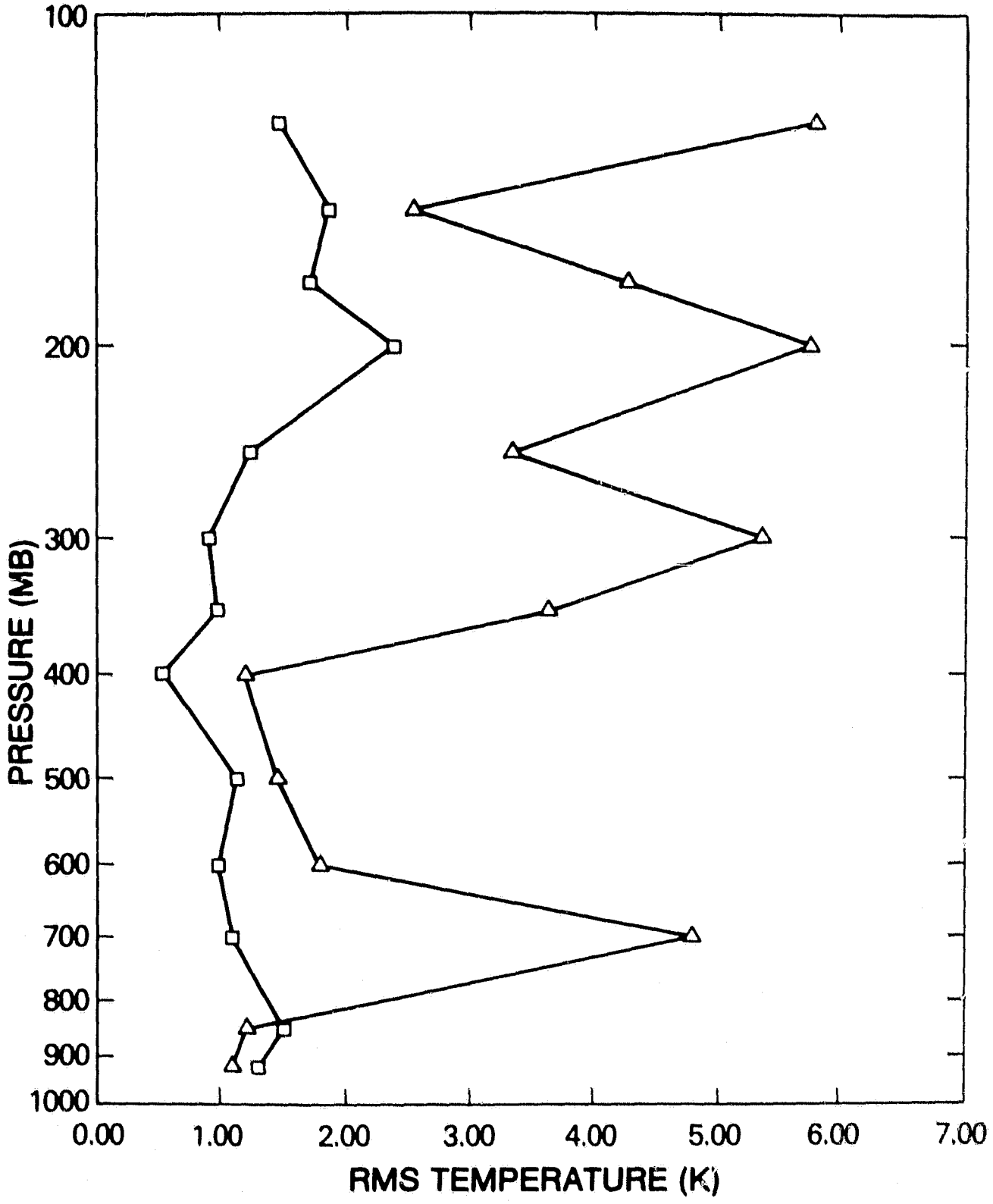

Figure 6. RMS temperature residuals (simulated sounding – "ground truth"), where VAS retrievals were statistically conditioned to expect vertical structure determined by either: (Δ) the "global" NOAA32 or (□) the "local" NSSL6 radiosonde sets.

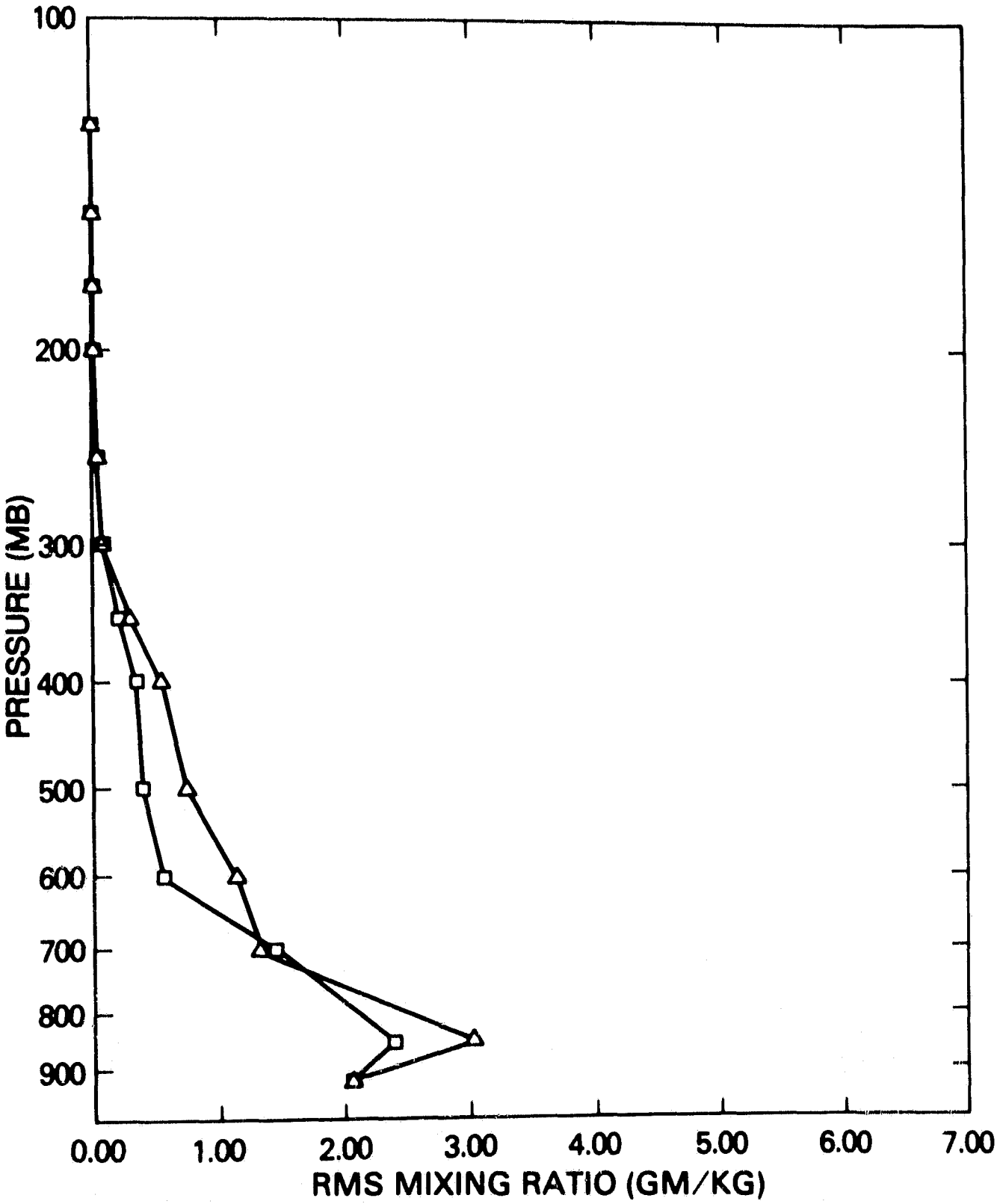

Figure 7. RMS mixing ratio residuals, where VAS retrievals were statistically conditioned to expect vertical structure determined by either: (△) the "global" NOAA32 or (□) the "local" NSSL6 radiosonde sets.

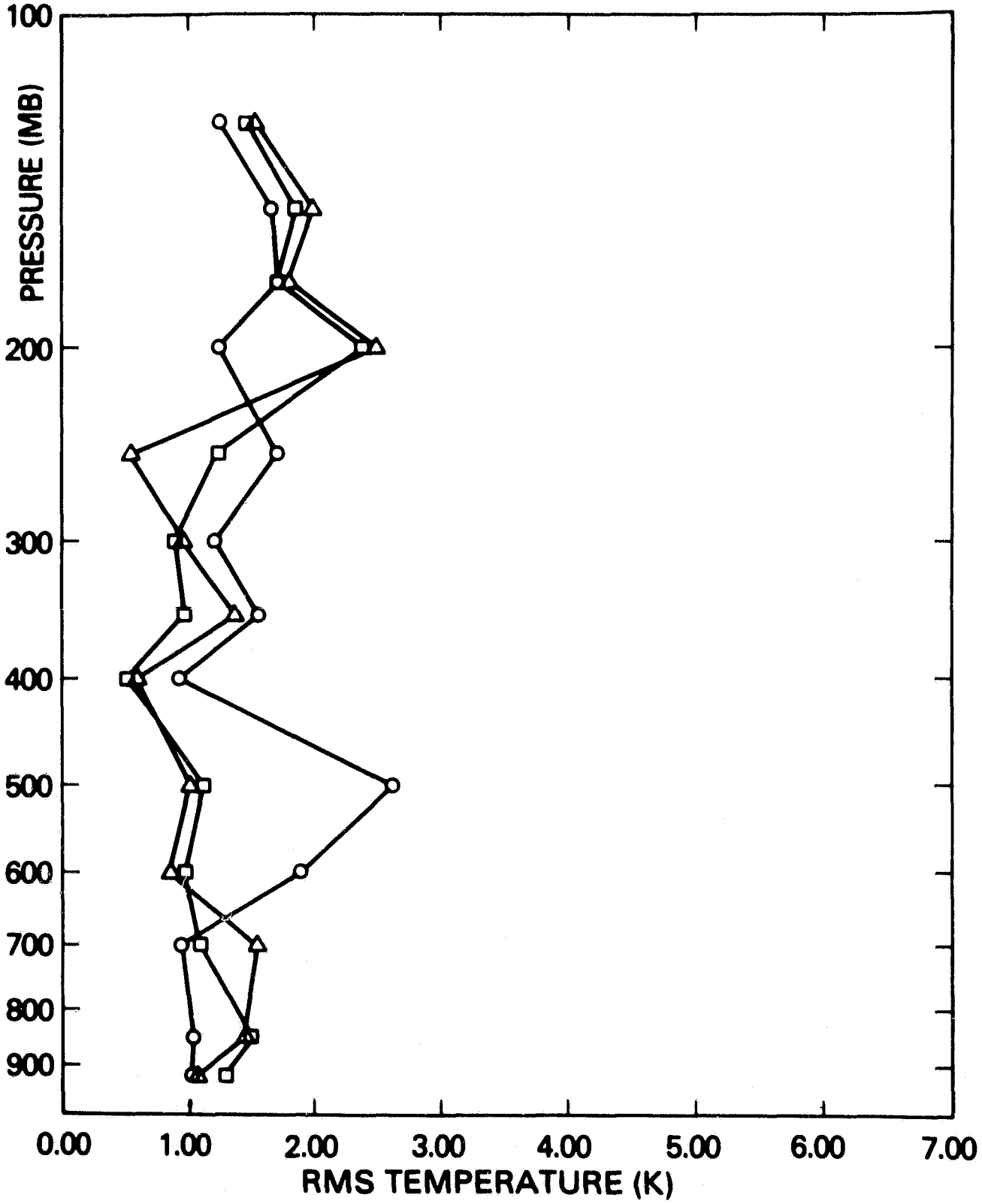

Figure 8. RMS temperature residuals using: (□) all, (△) "wet" and (○) "dry" SFOVs from the "local" NSSL6 training set to test even more detailed statistical conditioning of the simulated VAS soundings.

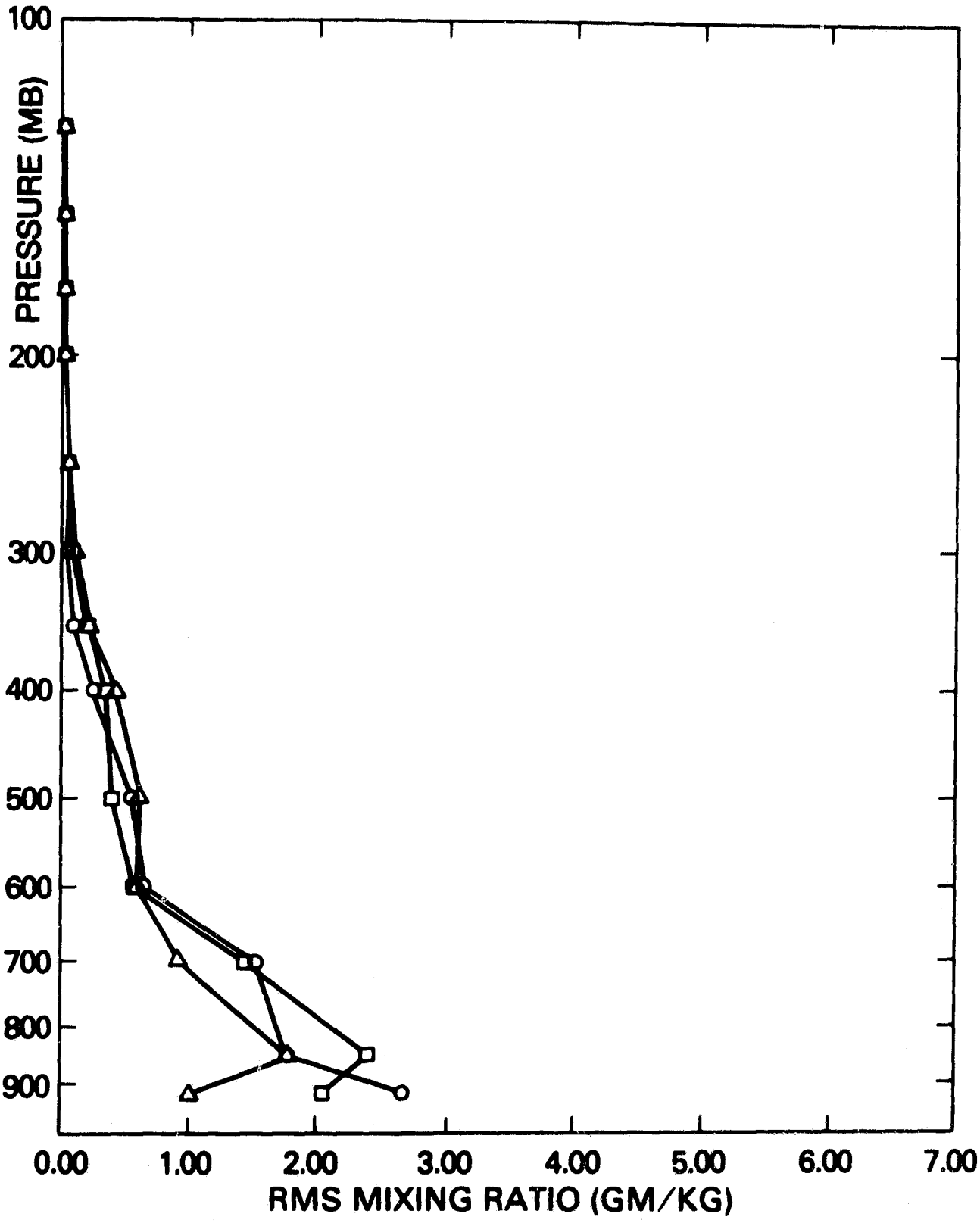

Figure 9. RMS mixing ratio residuals using: (□) all, (△) "wet" and (○) "dry" SFOVs from the "local" NSSL6 training set to test even more detailed statistical conditioning of the simulated VAS soundings.

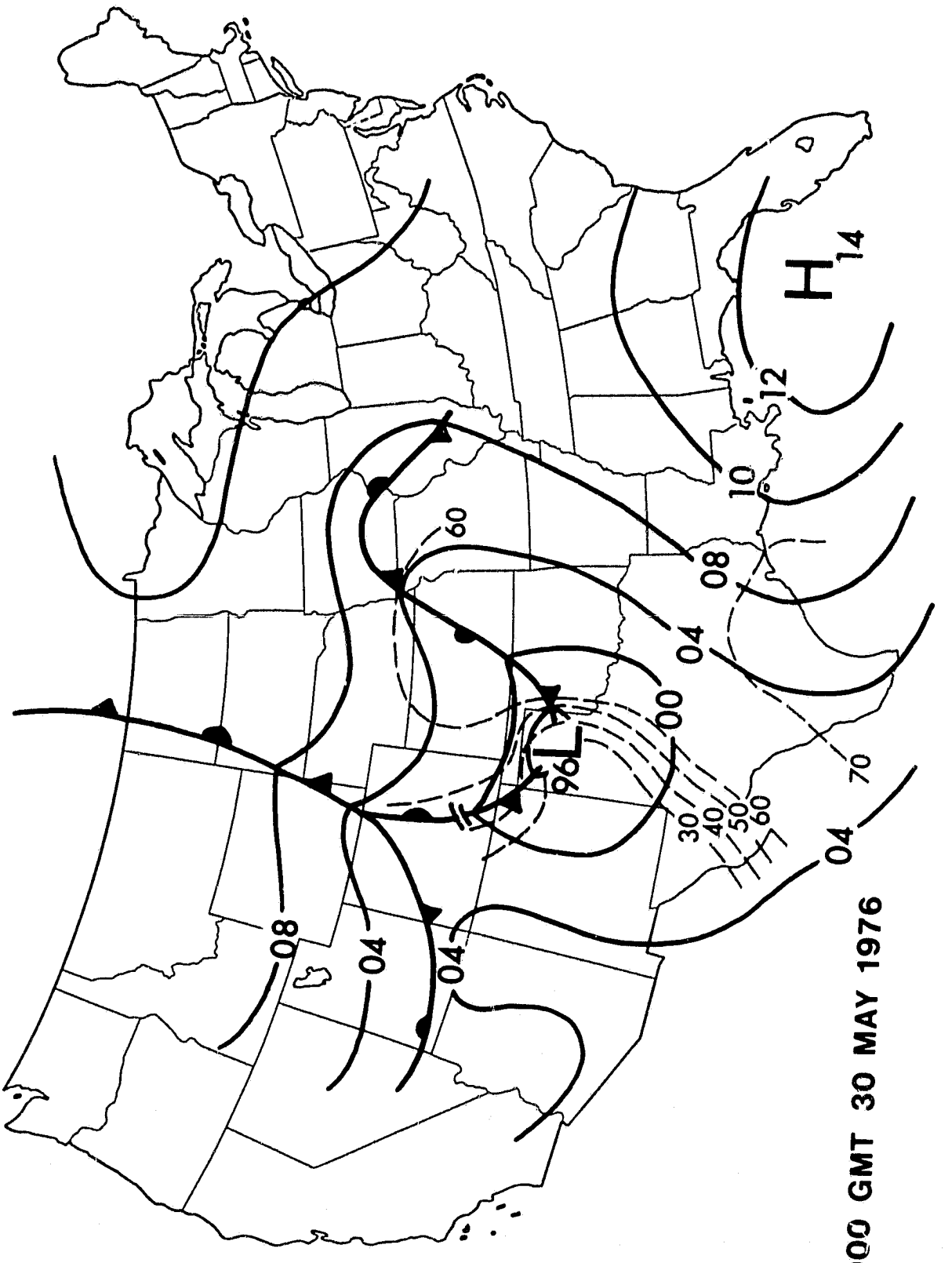

Figure 10. NWS surface analysis depicting pressure (mb) and dewpoint temperature (°F) at 0000 GMT 30 May 1976.